INFN/AE - 65/2
10 Dicembre 1965

ANTIPROTON-PROTON ELASTIC AND INELASTIC TOTAL CROSS SECTIONS BETWEEN 57 AND 178 MeV

U. Amaldi jr.[*], B. Conforto, G. Fidecaro, H. Steiner[**]
CERN Geneva

G. Baroni, R. Bizzarri, P. Guidoni, V. Rossi
Istituto di Fisica dell'Università - R o m a
Istituto Nazionale di Fisica Nucleare - Sezione di Roma

G. Brautti, E. Castelli, M. Ceschia, L. Chersovani, M. Sessa
Istituto di Fisica dell'Università - T r i e s t e
Istituto Nazionale di Fisica Nucleare - Sezione di Trieste

(*) Now at Istituto Superiore di Sanità, Rome.

(**) J.S. Guggenheim fellow on leave of absence from the University of California, Berkeley, Cal.

Errata - corrige

1. Page 11

Due to a numerical error the cross-sections at 57.26 MeV quoted in table V have been overestimated by about 5% the correct values being

σ_0	σ_2	σ_4	σ_6	σ_a	σ_i	σ_s	σ_t
24.6±2.0	61.2±3.2	66.5±3.4	5.7±0.9	133.4±5.0	158.0±5.5	82.8±3.8	240.8±7.1

The corresponding points in fig. 5 and 6 are incorrect by the same amount.

2. Page 13, line 11

Instead of

.... the various charged multiplicity of ....

read

.... the various charged multiplicities and the average multiplicity of ....

Summary.

About 25000 interactions of antiprotons of kinetic energy between 57 and 178 MeV have been measured in a hydrogen bubble chamber. Elastic and inelastic total cross sections have been determined at 15 values of the antiproton energy. The results have been compared with theoretical predictions.

R i a s s u n t o.

Circa 25000 interazioni di antiprotoni di energia cinetica tra 57 e 178 MeV sono state misurate in una camera a bolle a idrogeno.

Si sono determinate le sezioni d'urto totali elastica ed inelastica per 15 valori dell'energia dell'antiprotone. I risultati sono stati confrontati con le previsioni teoriche.

1. - Introduction.

The interaction of low energy antiprotons on protons has been studied by various authors by means of different detection techniques. Counter detectors, capable of separating the elastic from inelastic reactions have been used by Coombes et al [1] down to 133 MeV kinetic energy of the incident antiproton. More recent transmission measurements by U. Amaldi et al.[2] yielded the total cross section down to about 160 MeV. At lower energies the use of counter detectors becomes impractical, both because of the small intensity of the antiproton beams and the increasing importance of energy losses and multiple Coulomb scattering in the target. Propane [3] and hydrogen [4] [5] bubble chambers have been used to extend the measurements at lower energy. With the hydrogen bubble chamber technique Cork et al [4] have measured the elastic and inelastic cross sections from 45 to 245 MeV, and Loken and Derrick [5] the annihilation and charge exchange cross sections from 25 to 80 MeV. The elastic scattering cross section can also be measured using nuclear emulsions as detectors [6] [7]. This technique has been recently used by Hossain and Shaukat [7] to measure elastic scattering cross sections from 5 to 60 MeV.

The aim of the present experiment is to measure the $\bar{p}$-p cross sections in the energy region below 200 MeV with higher energy resolution and better statistical accuracy. The Saclay 81 cm hydrogen bubble chamber has been exposed to a separated antiproton beam from the CERN P.S. (CPS). About 25000 interactions of antiprotons of kinetic energy between 57 and 178 MeV have been measured. Elastic, inelastic and total cross sections have been determined at 15 different values of the $\bar{p}$ kinetic energy. The energy resolution (half width at half height) varies from ± 10 MeV at 57 MeV to ± 5 MeV at 177 MeV.

Results for the inelastic and the total elastic (integrated over all angles) cross sections are given in this paper. Angular distributions for elastic and charge exchange scattering will be presented in forthcoming papers. A preliminary account of this work has already been published [8].

2. - Beam and exposure.

The antiprotons were produced in a Be target at 11.25° by the circulating beam of the CPS and were transported to the 81 cm Saclay hydrogen bubble chamber (HBC) by means of the separated beam transport system, described in full detail elsewhere [9], which was operating at the CERN P.S. in 1961. The mass separation was obtained in two stages with two electrostatic separators [10]. The calculated contamination of pions and muons at the chamber

was less than 10^{-3} per antiproton. This has been confirmed by the film scanning. Momentum calibration of the beam has been obtained with a high precision (±0.02%) by means of two independent techniques: wire measurements and the time of flight of protons and deuterons in the beam.

Four exposures of the HBC have been made, covering the energy interval from 178 to 0 MeV. Since the antiproton intensity dropped very rapidly below 600 MeV/c, the beam momentum was set near this value and the antiprotons were moderated down to the required energy by means of absorbers. The first exposure was made mainly to study the annihilation of antiprotons at rest ([12]). A copper absorber 21.8 g/cm² thick was placed inside the vacuum tank just outside the chamber window in order to have the antiprotons stopping in the center of the chamber. In the second exposure the copper absorber had a thickness of 13.2 g/cm². In the third exposure 3.97 g/cm² of Al were placed outside the vacuum tank. No absorber was used in the fourth exposure.

The relevant information concerning the four exposures is collected in Table I. The

T A B L E I

Exp.	Momentum of the beam (MeV/c)	Momentum at the HBC (MeV/c)	Absorber and windows (g/cm²)	Beam conditions inside HBC at Hydr.	
				Kin. En. (MeV)	Momentum (MeV/c)
I a	615.5	609.0	21.8 Cu +	85.1	408.6
I b	612.8	606.2	1.75 Al	82.5	402.0
II a	615.5	609.0	13.2 Cu +	125.1	500.4
II b	612.8	606.2	1.75 Al	123.2	496.3
III	612.8	606.2	3.97 Al+ 1.75 Al	156.0	563.1
IV	643.7	637.3	1.75 Al	189.6	625.9

momentum of the beam for each exposure is shown in column 2. It should be noted that the pictures of both the first and second exposure have been taken in two different runs with two slightly different beam momenta. The momentum of the antiprotons before they enter the HBC vacuum tank is shown in column 3. It has been calculated from the values of the second column taking into account the slowing down in the material traversed by the antiprotons (four Mylar windows, 165 cm of air and the two scintillation counters which were used as monitors). The energy and momentum of the antiprotons entering the hydrogen of the bubble chamber are shown in the last two columns. They have been calculated taking into account the slowing down in the absorbers and in the chamber and vacuum tank walls (6.5 mm. of Al).

Since the magnetic field of the chamber strongly bent the low momentum particles before they entered the hydrogen, the HBC could not be at beam height. A magnet was placed in front

of the chamber to bend upwards the antiprotons to be injected in the HBC. The position of the chamber was chosen to have in the first exposure the antiprotons stopping in the center of the chamber with the maximum magnetic field (21 kgauss). In the other three exposures the magnetic field was lowered to 16 kgauss and the current in the injecting magnet varied in order to maximize the track length in the chamber. The antiproton mean trajectories inside the chamber are sketched in Fig. 1 for the four exposures.

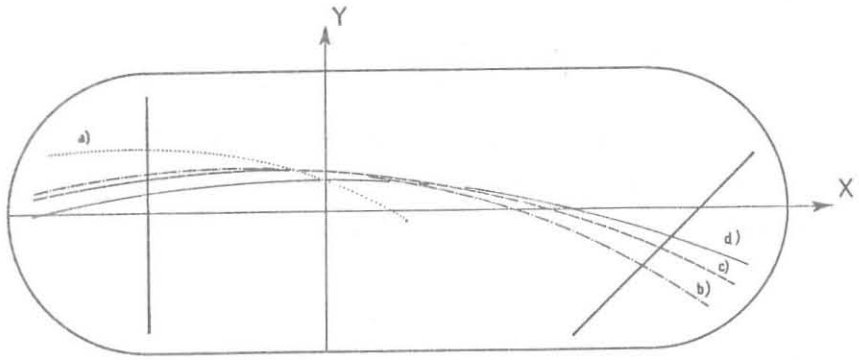

Fig. 1

Antiproton mean trajectories inside the chamber for the four exposures. At the entrance fiducial plane the momenta are respectively:

a) 363.5 MeV/c, b) 474.1 MeV/c,
c) 542.9 MeV/c, d) 609.7 MeV/c.

The time duration of the CPS burst during the experiment was about 1 ms, total width at half height. However the burst had a long tail (~ 5 ms) which contained about 5% of the intensity. An antiproton track belonging to this tail appears much lighter than the tracks of antiprotons on time. The problems connected with these tracks are discussed in Section 3.

3. - Scanning, measurements and selection of the events.

The film has been scanned for all the antiproton interactions. Antiprotons were easily distinguished from the very small contamination of mesons because of their higher ionization and also , since they lose more energy in the absorbers, because of their smaller radius of curvature. The interactions were classified into three groups:

a) annihilations into charged mesons: the antiproton disappears and an even number of charged mesons is produced;

b) zero-prong events: the antiproton disappears and no charged track is produced. These events are due either to annihilation into neutral mesons or to the charge exchange reaction $\bar{p} + p \rightarrow \bar{n} + n$;

c) elastic scattering events: the antiproton reemerges from the interaction point and a recoil proton is sometimes visible.

By double scanning of a fraction of the film the scanning efficiency was found to be 99% for annihilation events and 98% for zero-prong events. The scanning efficiency for elastic scattering events obviously depends upon the scattering angle. Details are given in Section 4.

For all the recorded events the interaction points have then been measured, together with two points on the incoming antiproton track, on at least two of the three stereoscopic views. In order to determine the total track length scanned, the non interacting tracks have also been measured every ten pictures (every twenty in a fraction of the film). The measurements were done on projected images of the film at about life size magnification. The typical measuring errors on the projected points were 0.2 mm. Helices have been fitted to the measured antiproton tracks, both the interacting and non interacting ones.

A fiducial volume of interaction has been defined by an entrance fiducial plane and an exit fiducial plane. The position of these planes with respect to the chamber is shown in Fig. 2 together with the reference system used. Both planes are parallel to the z axis, which

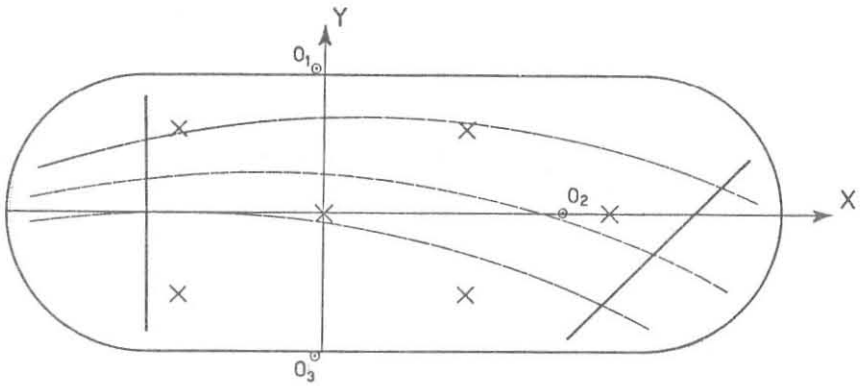

Fig. 2

Orthogonal projection on the back side of the front glass of the fiducial marks X, the cameras O_1, O_2 and O_3, the entrance (x = -18.5 cm.) and exit (y = x -35 cm) fiducial planes. The mean trajectory for the third exposure is drawn together with the two limit-trajectories.

is perpendicular to the chamber windows. These fiducial planes have been chosen in such a way that at least 3 cm of track are visible outside the fiducial volume. To completely determine the interaction volume a beam area on the entrance fiducial plane and an acceptance cone about the beam direction have been defined. Only tracks crossing the beam area within the acceptance cone have been retained. This ensures that:

i) the accepted tracks have entered the chamber going through the chamber window;

ii) the accepted tracks stay well inside the illuminated volume of the chamber before intersecting the exit fiducial plane;

iii) since the acceptance cone has an aperture of at most $6 \cdot 10^{-2}$ sr the probability of accepting an antiproton which has lost a large fraction of its energy through interactions in the moderator is negligible.

To apply the above mentioned criteria the intersection of each track with the entrance fiducial plane has been determined and the following quantities computed:

- the y and z coordinates of the entrance point (y_o and z_o);
- the dip angle β;
- the angle α between the projection of the track on the xy plane and the x axis.

The beam area is defined by placing limits on y_o and z_o and the acceptance cone by limits on α and β. In table II the limits used for the four exposures are shown together with

TABLE II

Exp.	Y min. (cm)	Y max. (cm)	$\bar{Y}$ (cm)	Z min. (cm)	Z max. (cm)	$\bar{Z}$ (cm)	α min. (rad)	α max. (rad)	$\bar{\alpha}$ (rad)	β min. (rad)	β max. (rad)	$\bar{\beta}$ (rad)	% rejected
I	0.0	8.0	6.5	12.0	20.0	16.0	-0.11	0.09	-0.02	-0.15	0.15	0.00	50.4
II	0.0	7.5	4.0	12.0	20.0	16.0	0.00	0.21	0.10	-0.13	0.13	0.00	15.0
III	0.0	7.5	3.5	11.0	21.0	15.7	0.03	0.20	0.11	-0.10	0.10	0.00	8.5
IV	-2.5	6.0	2.0	14.0	18.5	16.0	0.06	0.20	0.14	-0.06	0.06	0.00	4.8

the average values of the same quantities. The distribution of these quantities as determined on 3705 tracks from exposure III is shown in Fig. 3 both for the interacting (full line) and the non interacting (dotted line) tracks. The arrows indicate the limits of acceptance. It is seen that, at least within these limits, there is no significant difference between the distributions of interacting and non interacting tracks. The same is true for all the exposures.

The percentages of events rejected through these criteria are shown in the last column of table II. This percentage is of course larger the thicker is the moderator used, because of multiple Coulomb scattering in the moderator itself, and is anomalously large for exposure I because the beam was entering with a very high $\bar{y}_o$. Very asymmetric limits had to be placed on y_o to exclude tracks which had entered the HBC hitting the upper edge of the window.

In table III we report for each exposure the average length of non interacting tracks $\bar{\ell}$, the total track length used ℓ_t and the total number of interactions n_t accepted. In exposure I only the first 12 cm of track have been used for cross section measurements.

Particular attention should be devoted to the fact that the time distribution of the beam has a tail of late particles. Since these particles produce very thin tracks, the relative detection efficiency for late interacting and non interacting tracks could in principle be different from the analogous quantity for the on time events. To check this point the late tracks have been recorded separately. About 5% of the events were of this type. The ratio (number of events)/(total track length)has been computed separately for the on time

events and the late particles. The two ratios came out equal within the statistical error. After this check, late and on time tracks have been treated on equal footing in the determination of the cross sections.

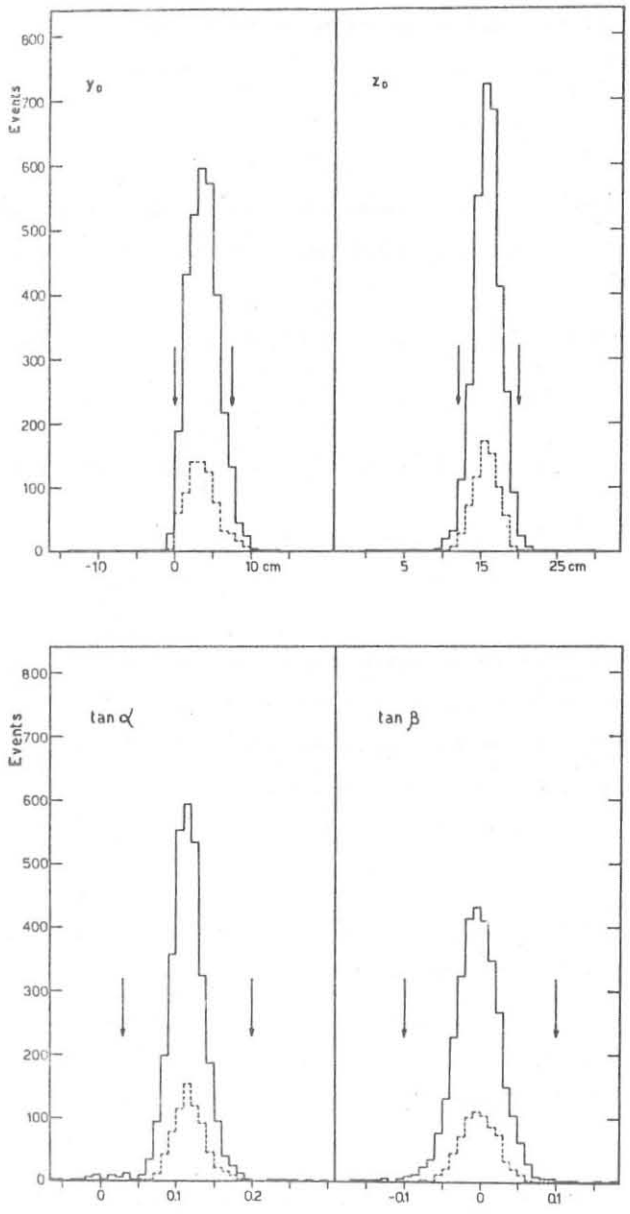

Fig. 3

Distributions of the four quantities y_0, t_0, tan α, tan β at the entrance fiducial plane for interacting (full line) and non interacting (dotted line) tracks in the third exposure; the arrows indicate the limits of acceptance.

4. - Energy determination and efficiency corrections.

The density of the liquid hydrogen in the Saclay HBC has been measured by the CERN - Saclay Collaboration to be $(625 \pm 1)\ 10^{-4}$ g/cm³ [13]. From the known values of the beam momentum inside the HBC at the hydrogen (Table I) we can then compute the average energy of the antiprotons at the entrance of the fiducial volume (Table IV). For the exposures II, III and IV the average energies at the exit of the fiducial volume can also be computed and are shown in the table. It appears that the whole range of energy up to 180 MeV is covered, with some overlap, by the four exposures.

TABLE III

Exposure	I	II	III	IV
$\bar{\ell}$ (cm.)	10	53	54	55
ℓ_t (km.)	0.48	11.5	13.1	11.9
n_t	411	8641	8541	7267

TABLE IV

Exposure	I		II		III	IV
	a	b	a	b		
Entrance Energy (MeV)	67	62	112	110	144	178
Exit Energy (MeV)	---	---	54	50	102	144

In exposure I the antiprotons stop in the chamber. Their average residual range from the entrance in the fiducial region, as computed from the known beam momentum is expected to be 29 cm. The experimental distribution of the length of 3532 annihilating tracks from exposure I is shown in fig. 4. If allowance is made for in flight annihilations this distribution results to be approximatively gaussian. The average range is 28 cm. in good agreement with the expected value. The r.m.s. spread is ± 5 cm. of hydrogen. This spread is the same for all energies indipendently from the thickness of material traversed by the beam. The corresponding momentum spread of the beam is $\Delta p_o/p_o = 0.85\%$ at 615 MeV/c, in good agreement with the beam design data. However after the slowing down through the moderator and the hydrogen the momentum spread increases: if we call p_o the initial momentum, we get at a momentum p,

$$\Delta p = \left[\left(dp/dx\right)_p \Big/ \left(dp/dx\right)_{p_o}\right] \Delta p_o \approx (p_o/p)^{2.6}\, \Delta p_o$$

For each interaction the arc length s of the incoming antiproton track from the entrance fiducial plane to the interaction point has been determined. The events have been grouped according to the value of s in intervals of 10 cm each. The average energy of each group is equal to the known energy of the beam at the entrance minus the energy lost in the liquid hydrogen up to the center of the interval. The distribution of residual ranges is the superposition of a gaussian distribution due to the beam spread with a flat rectangular distribution having the size of the chosen interval. The resulting distribution (not gaussian) has a full width at half height of 14 cm of liquid hydrogen. The distribution in energy inside each interval is more complicated and its width and shape depend upon the energy. Three typical energy distributions normalized to the same arbitrary height are shown on the abscissa axis of fig. 5.

The momentum of the interacting tracks could also be determined by measuring the curvature of the incoming antiprotons. The above described procedure however has been preferred because the error of a measurement of curvature strongly depends on momentum and track length, and furthermore because the resulting momentum error is larger than the momentum spread of the beam, except for the longest tracks in exposure II.

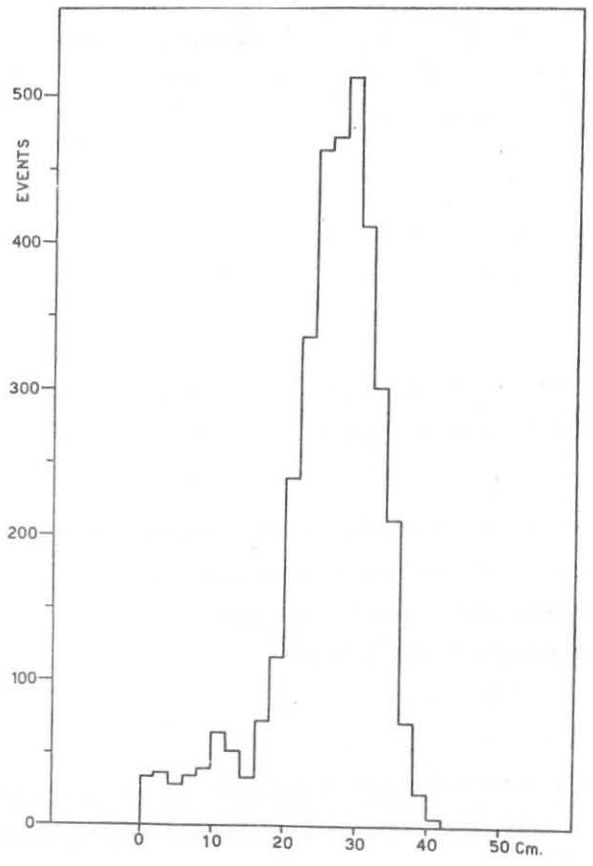

Fig. 4

Track length distribution of annihilating antiprotons in the first exposure.

A sistematic bias could be introduced by the presence of a tail of beam tracks having an energy considerably smaller than the average beam energy. A stopping antiproton in fact always annihilates at the end of its range while an average beam track, 50 cm long, has about a 20% probability of annihilation. A small contamination of stopping antiprotons in the beam tracks could then cause a serious overestimation of the annihilation cross section. We expected this effect to be negligible since all the processes by which an antiproton can lose a large amount of its energy without being scattered out of the beam are very improbable. This is confirmed by radius of curvature measurements. As the curvature for a stopping track is very different from that of a 50 MeV (or more) antiproton, even with rough curvature measurements we cam set an upper limit of 1% on the contamination of stopping antiprotons in the in flight events.

Before computing cross sections we must correct the observed number of events for possible detection inefficiencies. The observed number of annihilation and zero-prong events has simply to be increased by 1 and 2% respectively to take into account scanning losses. The probability of detection of an elastic scattering decreases rapidly with decreasing deflection angle. To avoid very large efficiency corrections, after having measured all the detected events, we retained only those with a laboratory scattering angle larger than 7°. To obtain the nuclear elastic scattering cross section from these events, the following corrections were applied:

a) the observed number was increased by 2% since the scanning efficiency for these events, as determined by double scanning, is 98%;

b) events with a laboratory scattering angle between 7° and about 18° can be missed at the scanning if the plane of scattering makes a large angle with the plane of the front glass of the chamber. By requiring the distribution of the normal to the scattering plane around the direction of the incident particle to be isotropic, we can estimate this loss to be about 3%;

c) the cross section for Coulomb scattering at laboratory angles larger than 7° has been subtracted. This cross section is only 1.2 mb at our lowest energy and rapidly decreases with energy;

d) the number of nuclear scatterings at angles smaller than 7° has been estimated extrapolating to 0° the measured differential cross sections by use of the optical theorem. The possible presence of a real forward scattering amplitude would not modify strongly this estimate: an increase of 20% in the differential cross section at 0° would produce an increase by only about 1% in the total elastic cross section.

5. - Results.

After applying these corrections, the cross sections for each interval can be obtained from the formula

$$\sigma = \frac{n}{\delta N L}$$

n = corrected number of events in the interval

δ = density of hydrogen

N = Avogadro's number

L = total length of track crossing the interval.

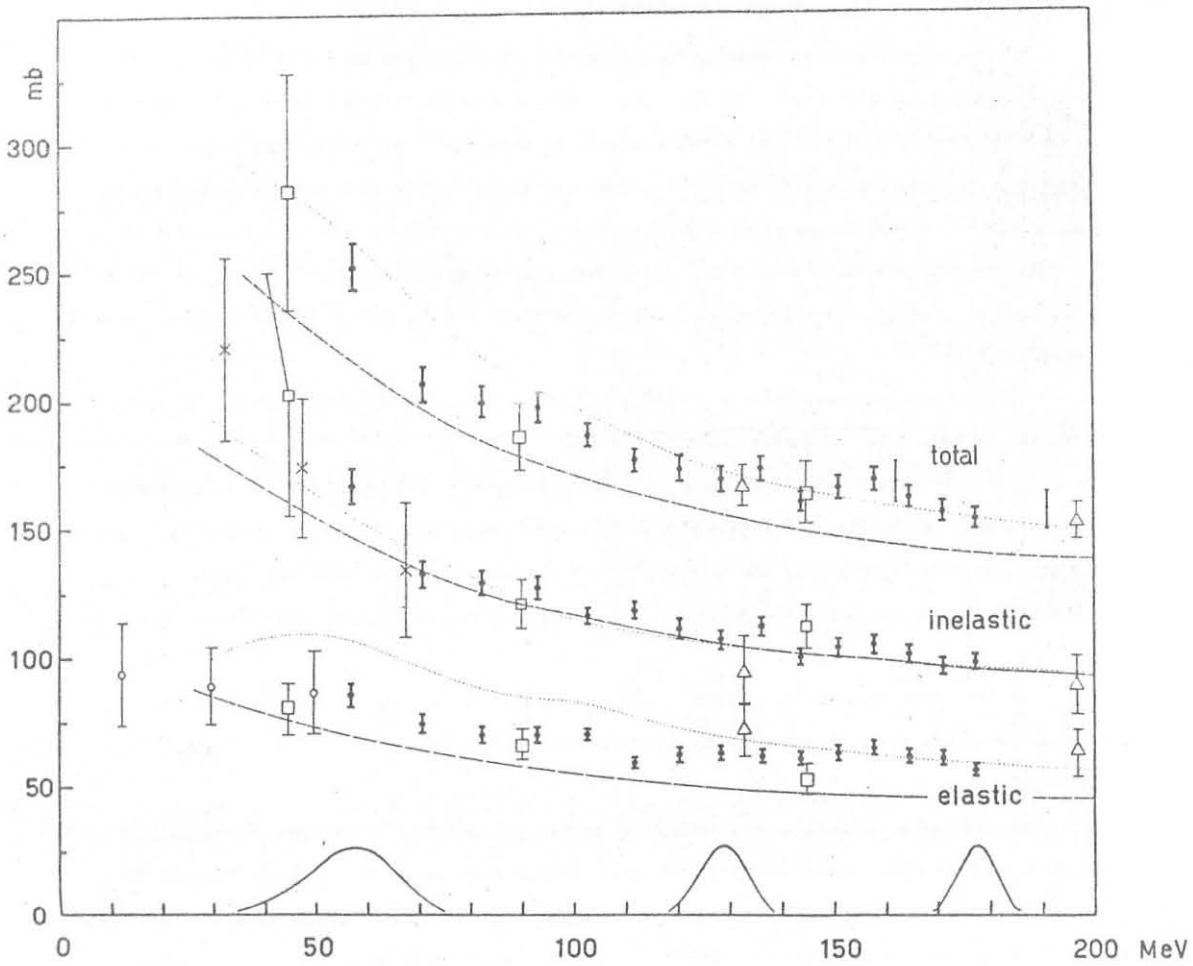

Fig. 5

Total, inelastic and elastic cross-sections versus energy.

This work; A. Hossain and M. Shaukat [7]; B. Cork et al. [4];

J.G. Loken and M. Derrick [5]; U. Amaldi et al. [2]; C. Coombes et al. [1].

The curves are theoretical calculations by M. Ceschia and A. Perlmutter (dotted line) and by J.P. Elagin et al. (dashed line).

Energy resolution curves for this experiment are shown on the abscissa axis.

TABLE V

Laboratory kinetic energy $\bar{T}_p$ (MeV)	Cross sections								$\rho=\sigma_s/\sigma_t$	M
	σ_0	σ_2	σ_4	σ_6	$\sigma_a=\sigma_2+\sigma_4+\sigma_6$	$\sigma_i=\sigma_a+\sigma_0$	σ_s	$\sigma_t=\sigma_s+\sigma_i$		
57.26	25.0±2.2	63.0±3.7	70.3±4.0	7.2±1.1	140.9±6.1	166.2±6.8	85.3±4.5	251.8±9.1	0.339±0.022	3.21±0.04
70.90	20.0±1.7	46.9±2.7	58.7±3.1	6.1±0.9	111.8±4.6	131.9±5.1	74.2±3.6	206.0±6.9	0.360±0.021	3.27±0.04
82.64	19.9±1.6	43.7±2.5	59.3±3.0	6.1±0.9	109.2±4.4	128.6±4.8	69.7±3.3	198.9±6.4	0.351±0.020	3.31±0.04
93.18	19.7±1.6	45.6±2.5	54.9±2.8	6.0±0.9	106.4±4.1	126.5±4.5	69.6±3.2	196.7±6.0	0.353±0.020	3.26±0.04
102.89	18.3±1.2	41.2±1.8	51.6±2.1	4.0±0.5	97.0±3.0	115.5±3.3	69.5±2.4	185.6±4.5	0.375±0.015	3.23±0.03
111.94	18.5±1.2	44.2±1.9	49.5±2.1	5.3±0.7	99.1±3.0	117.7±3.3	58.4±2.2	175.7±4.2	0.332±0.014	3.21±0.03
120.46	18.3±1.5	39.1±2.2	47.9±2.5	5.0±0.8	92.2±3.5	110.5±3.9	61.6±2.8	172.3±5.0	0.357±0.019	3.26±0.04
128.61	19.6±1.5	36.3±2.0	46.4±2.3	3.5±0.6	86.5±3.2	106.0±3.7	62.3±2.7	168.3±4.8	0.370±0.019	3.24±0.04
136.37	18.0±1.4	40.5±2.1	48.5±2.3	4.1±0.7	93.1±3.3	111.3±3.6	61.1±2.6	172.4±4.7	0.355±0.018	3.22±0.04
143.77	15.7±1.1	34.2±1.7	44.2±1.9	4.9±0.6	83.6±2.7	99.4±3.0	60.0±2.3	159.7±3.8	0.376±0.017	3.30±0.04
150.96	14.9±1.4	37.4±2.2	46.7±2.5	4.1±0.7	88.1±3.4	103.0±3.7	62.1±2.9	165.1±4.7	0.376±0.021	3.24±0.05
157.89	15.7±1.4	36.2±2.1	48.0±2.5	4.2±0.7	88.4±3.3	104.1±3.6	64.1±2.8	168.2±4.5	0.382±0.019	3.28±0.04
164.63	15.7±1.4	36.6±2.1	42.7±2.3	5.5±0.8	84.8±3.2	100.5±3.4	60.8±2.7	161.3±4.3	0.377±0.020	3.27±0.05
171.18	14.5±1.3	35.6±2.0	41.8±2.2	3.9±0.7	81.3±3.0	95.8±3.3	60.2±2.6	156.0±4.1	0.386±0.019	3.22±0.04
177.54	16.4±1.3	36.2±2.0	41.5±2.1	3.4±0.6	81.0±2.9	97.4±3.2	55.6±2.4	153.0±4.0	0.364±0.019	3.19±0.04

In Table V the results obtained for the following cross sections are shown

σ_0: 0-prong events

σ_2, σ_4, σ_6: annihilation into 2, 4, or 6 charged mesons

$\sigma_a = \sigma_2+\sigma_4+\sigma_6$: total of annihilations into charged mesons

$\sigma_i = \sigma_a+\sigma_0$: total of inelastic events

σ_s: elastic scattering

$\sigma_t = \sigma_s+\sigma_i$: total of all the events

as a function of the kinetic energy $T_{\bar{p}}$ of the incident antiproton in the laboratory system. Indicated errors are statistical. Also shown are ρ, the ratio of the elastic to the total cross sections, and M, the average charged multiplicity of annihilations with charged prongs.

In fig. 5, σ_t, σ_i and σ_s are shown versus $T_{\bar{p}}$ together with previous results in the same energy range. Energy resolution curves for three different energies are drawn, in arbitrary units, on the ascissa axis. The ratio $\rho = \sigma_s/\sigma_t$ does not vary significantly over our energy interval and is equal to about 0.37. The fact that ρ is smaller than 0.5 indicated that the angular momentum waves that contribute to the annihilation are only partially absorbed.

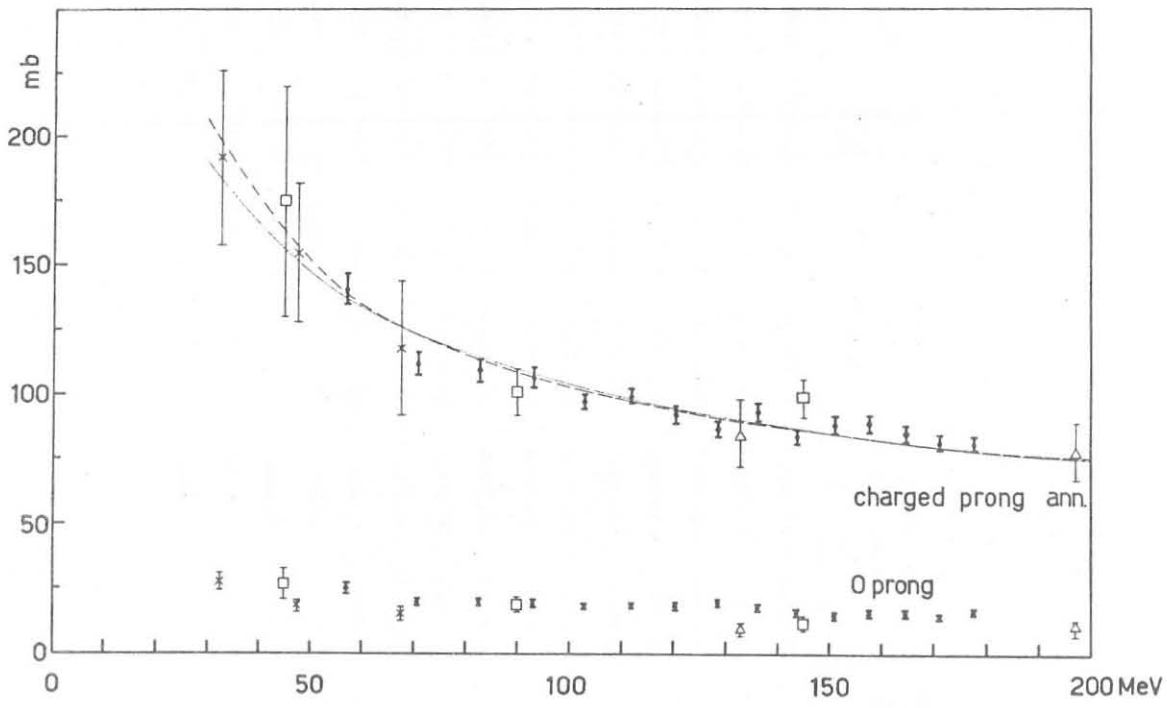

Fig. 6

Charged prong annihilation and zero prong cross-sections versus energy. ⊥ This work; ⊥ B. Cork et al.[4]; ⊥ J.G. Loken and M. Derrick[5]; ⊥ C. Coombes et al.[1]. The curves represent two fits to the annihilation cross-section assuming an energy dependence low of type $\pi(a+\lambda)^2$ (dashed line) and c (dotted line) respectively The best values are: $a = 0.90$ $F = 0.64\lambda_\pi$ and $c = 11.4$ $F = 8.1\lambda_\pi$

The knowledge of ρ and of the total cross section σ_t, allows one to make a statement on the minimum number of angular momentum waves contributing to the annihilation process([14]). The present data indicate that in all this energy range partial waves with values of the orbital angular momentum ℓ (and total angular momentum J) up to at least $\ell = 2$ (and $J = 2$), must contribute to the annihilation process.

In fig. 6 the cross sections for annihilations into charged mesons σ_a and for zero-prong events σ_o are separately shown. The annihilation cross section shows a smooth decrease with increasing energy. In fact the data can be quite well fitted assuming an energy dependence of the cross section of the type $A/\sqrt{T_{\bar{p}}} = B\lambda$ with A = 1037 mb MeV$^{1/2}$ and B = 11.4 F (λ being the wave number of the relative motion). The distribution of annihilation events into the various charged multiplicity of charged prongs do not show any appreciable variation over our energy range and are not different from those found from annihilation at rest ([15]).

To the cross section for 0-prong events contribute both annihilation into neutral mesons and charge exchange scattering. Except in a few cases in which an antineutron star is visible, the two classes of events are indistinguishable. The percentage of annihilations yielding all neutral products is known ([5])([15]) for antiprotons at rest (only S wave capture) to be 3.5%. We cannot however safely extrapolate this result to our energies. A state of only neutral pions is even under charge conjugation and at rest it can be produced only from the singlet S state, which has a small statistical weight. At our energies however contributions from the triplet states (^{3}P and possibly ^{3}F) are expected to be present. An increase of a factor 2 to 3 in the percentage of 0-prong annihilations cannot then be excluded ([16]). From our data the cross section for 0-prong events is about 20% of the cross section for annihilation into charged pions. We can then guess that the charge exchange cross section should account for 50 to 80 per cent of our 0-prong events.

6. - Comparison with theoretical models.

A very simple model of antinucleon-nucleon interaction has been considered by Koba and Takeda ([17]). They simply consider absorption and "shadow" scattering by a black sphere without any surrounding potential. If a is the radius of the black sphere the annihilation cross section should have the form $\sigma_a = \pi(a+\lambda)^2$. A good fit to our data is obtained with $a = 0.90$ F $= 0.64\ \lambda_\pi$. The predicted total cross section is however too low.

The effect of a real nucleon-antinucleon potential was first considered by Ball and Chew ([18]). They consider the N-$\bar{N}$ interaction as composed by two parts. A first part, completely analogous to the nucleon-nucleon interaction, can be described by a real potential which is obtained from the N-N potential taking into account the effect of charge conjugation. The second part describes annihilation and has no analogy in the N-N case. This second part is schematized by introducing a completely absorptive central core. Ball and Chew use then the WKB approximation in the calculations and the result is independent from the assumed core radius. The main difficulty with these calculations is that each angular momentum wave is assumed to be either completely absorbed or not absorbed at all. As a consequence the predicted

scattering cross section is larger than the absorption cross section. Experimentally the reverse is true: elastic scattering accounts only for about 37% of the total cross section.

A similar model for the N-$\bar{N}$ interaction has been used by Ceschia and Perlmutter [19]. They however avoid the use of the WKB approximation by explicitely solving under certain simplifying assumptions the Schroedinger equation. Free parameters then enter in the theory: the radius R of the absorptive core and the wave number of each partial wave inside the core. Ceschia and Perlmutter choose quite arbitrarily this wave number to be the same for all the partial waves. A reasonable fit to the data can then be obtained by choosing it to be one half of the free particle wave number and with a value of $R = \frac{2}{3} \lambda\!\!\!^{-}_{\pi}$. Their results are plotted as a dotted line in fig. 5. It appears that the predicted scattering cross section is higher than the measured one, the discrepancy being of about 20% below 100 MeV.

Similar calculations have been made by M.S. Spergel [20]. He minimizes scattering with respect to absorption by choosing the wave number of each partial wave inside the core in such a way to minimize the amount of reflection of each wave at the boundary. Core radii of 0.50, 0.55 and 0.60 $\lambda\!\!\!^{-}_{\pi}$ have been tried. A radius of 0.50 or 0.55 $\lambda\!\!\!^{-}_{\pi}$ can give the correct scattering cross section but the predicted annihilation cross section is than too low by 20÷25%. The use of a larger core radius would probably bring the annihilation cross section in agreement with measurements. However we cannot say if this can be done without changing too much the scattering cross section.

In conclusion it appears that the attempt to describe the annihilation process by simply introducing a completely absorptive core in addition to the real potential, can explain the annihilation cross section, provided a quite large core radius of about $2/3\ \lambda\!\!\!^{-}_{\pi}$ is assumed. The ratio ρ of the elastic to the total cross section however turns out to be always too large. This might be an intrinsic difficulty of the model due to the very sharp boundary of the absorptive region.

A different approach to the problem is to represent the interaction leading to annihilation by a suitably chosen imaginary potential. No theoretical prediction exists for the shape and strength of the potential which can then be chosen quite arbitrarily to fit the experimental data. This type of calculations has recently been performed by Nemirovskij and Strokov [21] who used an imaginary potential of the type $V = V_0\ e^{-r/c}$, with $V_0 = 4$ GeV, $c = 0.2\ \lambda\!\!\!^{-}_{\pi}$. Their results are also plotted in fig. 5 (dashed line). The agreement with the experimental data is only fair, the elastic scattering cross section being now underestimated by about 20%.

More recently Bryan and Phillips [22] have made calculations using an imaginary potential of the type $V_0/[1+\lambda \exp(ar)]$. Their preliminary results appear to give a good fit both to the elastic and inelastic cross sections.

7. - Acknowledgements.

We would like to thank Professor B. Gregory for his interest and contribution to the succes of the exposure.

We acknowledge the efficient running of the CERN P.S. and of the 81 cm Saclay HBC.

Part of the numerical computations has been performed at the computing centers of the Istituto Superiore di Sanità, Rome, of the Laboratori Nazionali di Frascati and of the University of Trieste.

Mrs. A. Rambaldi has contributed to the programming work.

REFERENCES

(1) C. A. Coombes, B. Cork, W. Galbraith, G. R. Lambertson and W. A. Wenzel: Phys. Rev. 112, 1303 (1958).

(2) U. Amaldi, T. Fazzini, G. Fidecaro, C. Ghesquière, M. Legros and H. Steiner: Nuovo Cimento 34, 825 (1964).

(3) L. E. Agnew, T. Elioff, W. B. Fowler, R. L. Lander, W. M. Powell, E. Segrè, H. M. Steiner, H. S. White, C. Weigand and T. Ypsilantis: Phys. Rev. 118, 1371 (1960).

(4) B. Cork, O. I. Dahe, D. H. Miller, A. G. Tenner and C. L. Wang: Nuovo Cimento 25, 497 (1962).

(5) J. Loken and M. Derrick: Phys Lett. 3, 334 (1963).

(6) G. Goldhaber, T. Kalogeropulos and R. Silberberg: Phys. Rev. 110, 1474 (1958). G. Baroni, G. Bellettini, C. Castagnoli, M. Ferro Luzzi, A. Manfredini: Nuovo Cimento 12, 564 (1959) A. G. Ekspong and B. E. Ronne: Nuovo Cimento 13, 27 (1959)

(7) A. Hossain and M. A. Shaukat: Nuovo Cimento 38,737 (1965).

(8) U. Amaldi Jr., B. Conforto, G. Fidecaro, H. Steiner, R. Tosi-Torelli, G. Baroni, R. Bizzarri, P. Guidoni, F. Marcelja, V. Rossi, A. Stajano, G. Brautti, E. Castelli, M. Ceschia, L. Chersovani and M. Sessa: Proceedings of the Siena International Conference on Elementary Particles (1963), vol. I, pag. 243.

(9) U. Amaldi, T. Fazzini, G. Fidecaro, C. Ghesquière, M. Legros and H. Steiner: Nuovo Cimento 30, 973 (1963).

(10) The separators have been kindly put at our disposal by the separator Group of the Padua Section of INFN.

(11) At the time the experiment has been performed the PS maximum intensity was $2 \cdot 10^{11}$ protons/burst.

(12) CERN - École Polytechnique and Oxford - Padua collaborations. We have used only a small fraction of the film obtained in this exposure.

(13) R. Armenteros: Private communication.

(14) W. Rarita and P. Schwed: Phys Rev. 112, 271 (1958).

(15) G. B. Chadwick, W. T. Davies, M. Derrick, J. H. Mulvey; D. Radojicic, C. A. Wilkinson, M. Cresti, S. Limentani, A. Loria, R. Santangelo: Proc. of the Aix-en-Provence Int. Conf. on Elementary Particles (1961), Vol. I, pag, 269.

(16) B. R. Desai: Phys. Rev. 119, 1390 (1960).

(17) Z. Koba and G. Takeda: Prog. Theor. Phys. 19, 269 (1958).

(18) J. S. Ball and J. F. Chew: Phys. Rev. 109, 1385 (1958).

(19) M. Ceschia and A. Perlmutter: Nuovo Cimento 33, 578 (1964).

(20) M. S. Spergel: University of Rochester report UR-875-24.

(21) P. E. Nemirovskii and Yu. F. Strokov: J. Expth. Theoret. Phys. (U.S.S.R.) 46, 1379 (1964); translated in Soviet Physics JETP 19, 932 (1964). See also Ju. P. Elagin, P. E. Nemirovskii, Ju. F. Strokov: Phys. Lett. 7, 352 (1963).

(22) R.A. Bryan and R.J.N. Phillips - Bull. Am. Phys. Soc. 10, 737 (1965) and private communications.